

## Characterizing the edge of chaos for a shear flow model

Lina Kim\* and Jeff Moehlis†

*Department of Mechanical Engineering, University of California, Santa Barbara, California 93106, USA*  
(Received 6 November 2007; revised manuscript received 21 August 2008; published 16 September 2008)

We characterize the edge of chaos, the boundary which separates initial conditions which lead to chaotic behavior from those which directly decay to the laminar state, for a nine-dimensional shear flow model. This boundary is the eight-dimensional stable manifold of an unstable periodic orbit, whose properties are characterized. Furthermore, we compute the probability that perturbations of a given energy will lead to transient chaos before decaying to the laminar state, or to a nontrivial attractor for a range of Reynolds numbers. Finally, we consider the relationship between the edge of chaos and linear transient growth, a mechanism which may trigger nonlinear effects that lead to turbulence in shear flows.

DOI: 10.1103/PhysRevE.78.036315

PACS number(s): 47.27.Cn, 47.15.Fe

### I. INTRODUCTION

The transition to turbulence in shear flows is a well studied but unsolved problem of great importance and interest [1,2]. Much of the theoretical interest in this problem derives from the fact that turbulence can occur despite stability of the laminar state. For example, linear stability theory predicts that shear flows such as plane Couette and pipe flow remain asymptotically stable for all Reynolds numbers [3]. However, in practice these flows can exhibit turbulent behavior, and the turbulence arises abruptly: it does not develop from laminar flow through a sequence of transitions to more and more complicated behavior [3]. Interestingly, for such flows, the governing equations can possess numerous branches of unstable steady or traveling wave states that arise from saddle node bifurcations [4–9]. Despite recent progress [9–13], the relationship between these three-dimensional solutions and turbulence has still not been clarified.

For a shear flow for which the laminar state is stable but (transient or sustained) turbulence coexists, one can ask if there is a boundary for which all initial conditions starting on one side will decay directly to the laminar state, and those on the other side will lead to (transient or sustained) turbulence. Furthermore, if there is such a boundary, what is its nature and geometry? Such questions were considered in Ref. [10] for a low-dimensional model for a parallel shear flow. For this model, the boundary between laminar and turbulent behavior was found by measuring the lifetime of an initial condition, i.e., the time it takes for an initial condition to laminarize. This boundary (called the edge of chaos), which separates transient chaotic and transient nonchaotic behavior, was found to be the stable manifold of an unstable periodic orbit (called the edge state), at least for moderate Reynolds numbers. Later, in Ref. [11], the edge of chaos for pipe flow was found to be the stable manifold of a relative attractor, and the edge state is dominated by streak and streamwise vortices.

This paper will focus on characterizing the edge of chaos for the nine-dimensional model for sinusoidal shear flow (SSF) from Refs. [14,15], which has trajectories that either directly decay to the laminar state, become transiently chaotic before decaying to the laminar state, or become transiently chaotic before moving towards a nontrivial attractor. We hope that this study will help to clarify the issues which we expect to be relevant for understanding the transition to turbulence in other shear flows. In Sec. II we introduce the model, compare turbulent statistics to direct numerical simulation (DNS) data from plane Couette flow (PCF), and define the energy in the system. The relevant behavior of the model and properties of the edge of chaos are described in Sec. III. We investigate the role of transient energy growth in determining whether or not initial conditions lead to transient chaos for this model in Sec. IV. Finally, in Sec. V, we give concluding remarks.

### II. SSF MODEL

We consider SSF for an incompressible fluid and choose a coordinate system such that  $x$ ,  $y$ , and  $z$ , respectively, correspond to the streamwise, wall-normal, and spanwise directions; see Fig. 1. The flow obeys the nondimensional equations

$$\frac{\partial \mathbf{u}}{\partial t} = -(\mathbf{u} \cdot \nabla) \mathbf{u} - \nabla p + \frac{1}{\text{Re}} \nabla^2 \mathbf{u} + \mathbf{F}(y), \quad (1)$$

$$\nabla \cdot \mathbf{u} = 0, \quad (2)$$

where  $\text{Re}$  is the Reynolds number. The time independent sinusoidal body force in the streamwise direction given by

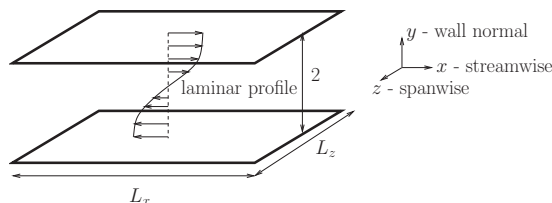


FIG. 1. Geometry for SSF.

\*lina@engineering.ucsb.edu

†http://www.me.ucsb.edu/~moehlis;

moehlis@engineering.ucsb.edu

$$\mathbf{F}(y) = \frac{\sqrt{2}\pi^2}{4\text{Re}} \sin\left(\frac{\pi y}{2}\right) \hat{\mathbf{e}}_x \quad (3)$$

results in the laminar profile

$$\mathbf{U}(y) = [\sqrt{2} \sin(\pi y/2), 0, 0], \quad (4)$$

which is linearly stable for all Re [3]. Free-slip boundary conditions

$$u_y = 0, \quad \frac{\partial u_x}{\partial y} = \frac{\partial u_z}{\partial y} = 0 \quad (5)$$

are imposed at  $y = \pm 1$ , and the flow is assumed periodic in the streamwise and spanwise directions, with lengths  $L_x$  and  $L_z$ , respectively.

A nine-dimensional model, obtained by Galerkin projection of Eq. (1) onto important flow structures, was introduced in Ref. [14]; see also Ref. [15]. Specifically, the velocity is expanded as

$$\mathbf{u}(\mathbf{x}, t) = \sum_{j=1}^9 a_j(t) \mathbf{u}_j(\mathbf{x}), \quad (6)$$

where the amplitudes  $a_j$  are real and the modes  $\mathbf{u}_j$ , given in Ref. [14], are orthogonal under the standard inner product. Physically,  $\mathbf{u}_1$  is a mode representing the laminar profile given in Eq. (4),  $\mathbf{u}_2$  is a streak mode,  $\mathbf{u}_3$  is a downstream vortex mode,  $\mathbf{u}_4$  and  $\mathbf{u}_5$  are spanwise flow modes,  $\mathbf{u}_6$  and  $\mathbf{u}_7$  are normal vortex modes,  $\mathbf{u}_8$  is a three-dimensional mode, and  $\mathbf{u}_9$  gives a modification to the laminar profile. Inserting Eq. (6) into Eq. (1) and projecting, we obtain a set of nine coupled, nonlinear ordinary differential equations. This model generalizes the eight-mode model of Ref. [16], with the main improvement being the inclusion of a mode which represents the lowest order modification of the mean profile (4); other modes from the eight-mode model are modified slightly so that they can couple to this new mode. The transition to turbulence for this nine-mode model is subcritical, i.e., although the laminar state is stable for all Re, it is possible to get turbulentlike behavior for some Re. Furthermore, if there is only transient turbulentlike behavior, the distributions of turbulent lifetimes, i.e., the duration of turbulence before decay to the laminar state, are exponential, in agreement with observations in many shear flows [14].

It is hoped that the knowledge gained from studying the edge of chaos for SSF will be relevant to the laminar-turbulent boundary dynamics for other shear flows. SSF represents a nontrivial shear flow whose geometry resembles that of PCF but with free slip boundary conditions which allow the modes  $\mathbf{u}_1, \dots, \mathbf{u}_9$  to be written in terms of trigonometric functions. In Fig. 2, we compare statistics of fluctuations from the laminar state for the stable periodic orbit for the nine-mode model with turbulent DNS data for PCF from Ref. [17], both at  $\text{Re}=400$  with  $L_x=1.75\pi$  and  $L_z=1.2\pi$ . For the wall-normal root mean square (RMS) fluctuations  $\sqrt{\langle v'^2 \rangle}$  and the Reynolds stress  $\langle u'v' \rangle$  the trend is the same in terms of the location of the peaks, but  $\langle u'v' \rangle$  for the nine-mode model is smaller by an order of magnitude. We note that the streamwise and spanwise RMS fluctuations differ more substantially for the two flows, which is consistent with the dif-

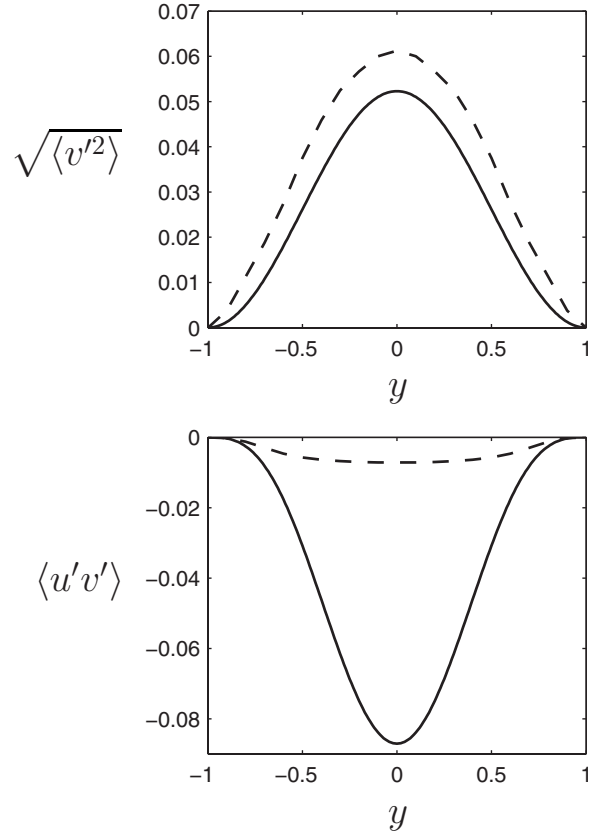


FIG. 2. Comparison of turbulent statistics for the nine-mode model for SSF (solid) and PCF with DNS data from Ref. [17] (dashed).

ferent boundary conditions. Nonetheless, the agreement in these quantities, and the work in Ref. [14] supports the idea that this nine-mode model is a good representation and captures essential behaviors of typical shear flows.

In the following, the energy in the system is taken to be the fluctuation energy with respect to the laminar profile, and is defined as

$$E \equiv (1 - a_1)^2 + \sum_{j=2}^9 a_j^2. \quad (7)$$

Note that the modes have been normalized so that the energy contained in a given mode is simply the amplitude of the mode squared. Throughout this paper, we consider a flow domain with  $L_x=1.75\pi$  and  $L_z=1.2\pi$ ; for the related system of PCF, these parameters correspond to the minimal flow unit, the smallest domain which is found numerically to sustain turbulence [18].

### III. THE EDGE OF CHAOS

#### A. The unstable periodic orbit associated with the edge

For this system, there is an asymptotically stable fixed point at  $a_1=1, a_2=\dots=a_9=0$  for all Re which corresponds to the laminar state. For  $\text{Re} \leq 335$  and  $515 \leq \text{Re} < 1000$ , this fixed point is the global attractor for this model, so that all trajectories will eventually end up at the laminar state fixed

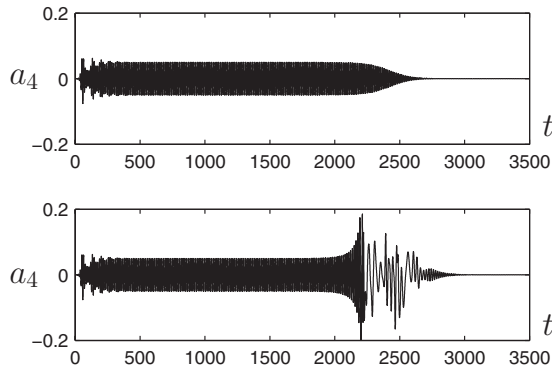


FIG. 3. Time evolution for the amplitude  $a_4$  for the nine-dimensional model at  $Re=300$  showing qualitatively different behaviors for two nearby initial conditions. The initial conditions for the top and bottom trajectories were kept constant with the exception of  $a_4(0)$ , which only differ from each other by a quantity of order  $10^{-15}$ .

point. Initial conditions for this range of  $Re$  exhibit two distinct behaviors: direct laminarization or a chaotic transient before decaying to the laminar state. This behavior coincides with the situation for the low-dimensional model considered in Ref. [10]. Figure 3 shows the evolution of amplitude  $a_4$  as a function of time at  $Re=300$  for two initial conditions near the laminar state, which in this figure corresponds to  $a_4=0$ . The top panel corresponds to a trajectory which visits near an unstable periodic orbit (UPO) before decaying to the laminar state, and the bottom panel corresponds to a trajectory which visits close to the same periodic orbit and undergoes transient chaotic dynamics before laminarization. As clarified below, the stable manifold of this periodic orbit separates initial conditions which directly laminarize from those which are transiently chaotic. Thus, the UPO visited by such trajectories determines the edge of chaos.

The transient chaotic state in this system is associated with a chaotic saddle near which trajectories stay for a finite time before escaping. The duration of the chaotic transient is very sensitive to initial conditions and  $Re$  as indicated by the fractal nature of lifetimes [10,14,19], but the overall trend is that it increases with  $Re$ . Figure 4 shows a schematic diagram showing the UPO associated with the edge coexisting with the asymptotically stable laminar state fixed point and the chaotic saddle in phase space. The UPO is only unstable in one direction, therefore, the stable manifold is the surface which separates initial conditions which directly decay to the laminar state (such as the one labeled  $a$ ) from those which visit near the chaotic saddle before laminarizing (such as the one labeled  $b$ ).

Our method for finding the edge of chaos is similar to that used for a different model in Ref. [10]. The edge tracking algorithm starts out with a randomly chosen initial condition. One of the benefits of this algorithm is that it does not have to start with a particular type of initial condition, that is, the algorithm can find the edge of chaos when starting with an initial condition which either decays directly to the laminar state or shows chaotic behavior. We then systematically update that initial condition along a one-dimensional curve in phase space, near the laminar state fixed point, as follows: if

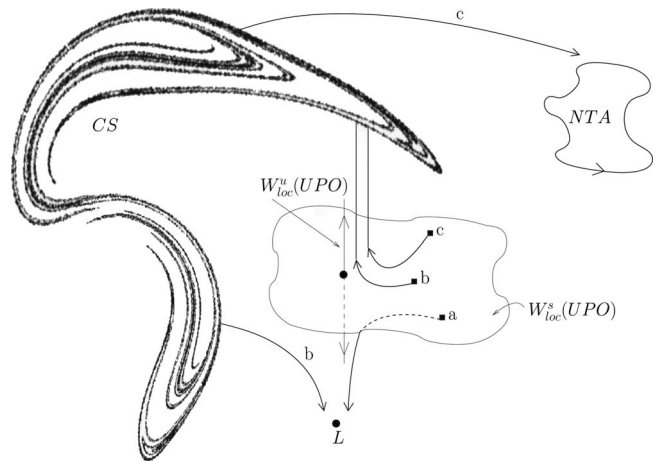


FIG. 4. A schematic diagram showing the laminar state ( $L$ ), the unstable periodic orbit (UPO) associated with the edge, the chaotic saddle ( $CS$ ), the nontrivial attractor ( $NTA$ ), and three initial conditions which exhibit qualitatively distinct dynamics. The UPO, represented as a dot, has a one-dimensional unstable manifold labeled  $W_{loc}^u(UPO)$  and an eight-dimensional stable manifold labeled  $W_{loc}^s(UPO)$ , which forms the edge of chaos. For  $Re \lesssim 335$  and  $515 \lesssim Re < 1000$ , the only attractor in the system is the laminar state fixed point and initial conditions either (a) decay directly to the laminar state (see top panel of Fig. 3) or (b) become transiently chaotic before decaying to the laminar state (see bottom panel of Fig. 3). For  $335 \lesssim Re \lesssim 515$ , initial conditions may tend towards a nontrivial attractor as in (c) and Fig. 10.

the trajectory directly decays to the laminar state, we take an initial condition on the curve further away from the laminar state, and conversely, if the trajectory shows transient chaos, we take an initial condition on the curve closer to the laminar state. The points further/closer to the laminar state fixed point are typically found by simultaneously varying up to three of the amplitudes  $a_j$ . By refining the initial conditions via a bisection rule, we find trajectories which spend more and more time in the neighborhood of the UPO whose stable manifold forms the edge.

Figures 5 and 6 show the UPO associated with the edge of chaos for this system which is visited by these trajectories. Indeed, it is found numerically with AUTO, a software program for numerical continuation bifurcation analysis [20], that this periodic orbit has only one unstable direction. Its eight-dimensional stable manifold separates initial conditions

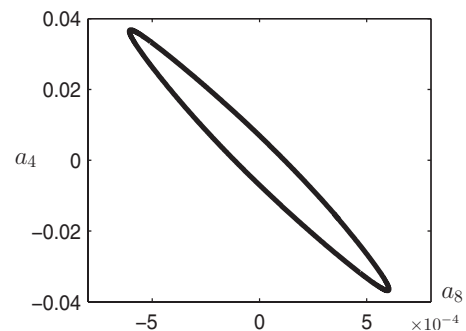


FIG. 5. The unstable periodic orbit associated with the edge of chaos for  $Re=400$  with period  $T=13.60$ .

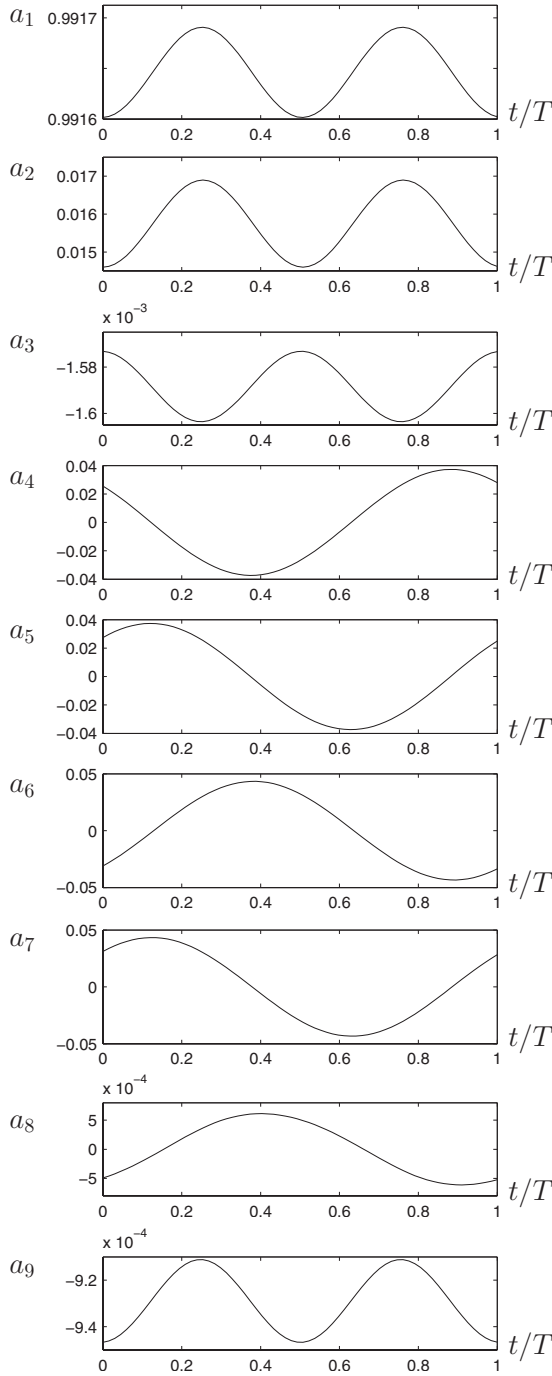


FIG. 6. Time series for the amplitudes of the edge periodic orbit for  $Re=400$  over one period.

which directly decay to the laminar state from those which exhibit transiently chaotic behavior, and forms the edge of chaos. We also confirmed that this remains the periodic orbit associated with the edge of chaos by finding the edge using the bisection method at other  $Re$ . Moreover, we verified that our edge tracking algorithm converges to the same orbit regardless of the initial conditions used to begin the bisection algorithm and the direction we choose for the one dimensional curve which intersects its stable manifold. We note that for  $Re \geq 250$ , this periodic orbit has the smallest mean perturbation energy of all the periodic orbits found for this

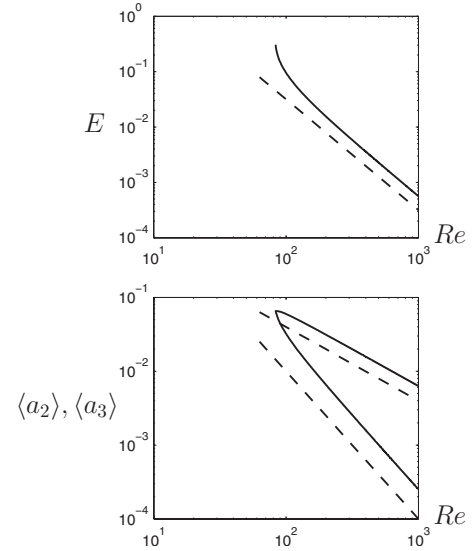


FIG. 7. The average values for the energy and the amplitudes corresponding to the streaks ( $a_2$ ) and streamwise vortices ( $a_3$ ) of the UPO associated with the edge of chaos as a function of  $Re$ . (top) The average energy of the UPO (solid) scales as  $Re^{-2}$  (dashed). A scaling analysis reveals that (bottom)  $\langle a_2 \rangle$  (upper solid curve) scales as  $Re^{-1}$  (upper dashed line) while  $\langle a_3 \rangle$  (lower solid curve) scales as  $Re^{-2}$  (lower dashed line).

system [14,15]. For  $Re \leq 250$ , the only periodic orbits with smaller mean perturbation energy arise in a bifurcation from this periodic orbit branch.

From Fig. 6, which shows the evolution of the modes for the UPO associated with the edge of chaos for  $Re=400$ , we see that there is a difference between the group of modes which represent the instability in the streaks and the three-dimensional flow  $S_A: \{a_4, a_5, a_6, a_7, a_8\}$  and the modes corresponding to the basic profile, streamwise vortices, and streaks  $S_B: \{a_1, a_2, a_3, a_9\}$ . In particular, the period of the modes in group  $S_B$  is twice that of the modes in group  $S_A$ . Furthermore, the modes in group  $S_A$  have larger peak-to-peak amplitudes than those in group  $S_B$ : the peak-to-peak amplitudes of the modes in group  $S_A$  are approximately 50–2500 times larger than the peak-to-peak amplitudes of the modes in group  $S_B$ , with the exception of the streak mode with amplitude  $a_2$  whose peak-to-peak amplitude was comparable to those of the modes in  $S_A$ . This implies that the dynamics of the unstable periodic orbit associated with the edge of chaos are dominated by the streak and streak instability modes.

Using AUTO [20], a scaling analysis was conducted by calculating the average values of the energy, streak amplitude, and streamwise vortex amplitude in the UPO associated with the edge of chaos; see Fig. 7. The average energy, streak and streamwise vortex modes scale as  $Re^{-2}, Re^{-1}, Re^{-2}$ , respectively. These scalings are different from comparable results found in Ref. [9] which finds that for the lower branch state for PCF, the amplitudes of the streaks and streamwise vortices scale as  $Re^0, Re^{-1}$ , respectively. A possible explanation for the difference in the scalings is the different boundary conditions for the two flows. However, we note that the ratio between the scalings of the vortices and streaks is the

same, i.e.,  $\frac{\langle a_3 \rangle}{\langle a_2 \rangle} \sim \text{Re}^{-1}$ , which indicates that for both PCF and the nine-mode model for SSF the streamwise vortices become relatively weaker as  $\text{Re}$  increases.

As noted in Ref. [15], the model for SSF is equivariant [21,22] with respect to the group  $D_2 \equiv \{Id, \mathcal{T}_{L_x/2}, \mathcal{T}_{L_z/2}, \mathcal{T}_{L_x/2, L_z/2}\}$ . These group elements respectively correspond to the identity element, translation by  $L_x/2$  in the streamwise direction, translation by  $L_z/2$  in the spanwise direction, and the application of both such translations. The action of  $\mathcal{T}_{L_x/2}$  on the unstable periodic orbit associated with the edge of chaos gives a time shift of half of a period; thus, this periodic orbit is (setwise) invariant under  $\mathcal{T}_{L_x/2}$ . The action of  $\mathcal{T}_{L_z/2}$  on this periodic orbit gives a distinct, symmetry-related unstable periodic orbit, which is also (setwise) invariant under  $\mathcal{T}_{L_x/2}$ . (The periodic orbit obtained by the action of  $\mathcal{T}_{L_x/2, L_z/2}$  on the original unstable periodic orbit is related to the latter one by a time shift of half a period.) Thus, there are two symmetry-related unstable periodic solutions, each with its own eight-dimensional stable manifold which forms an edge of chaos. By uniqueness of solutions backwards in time, these stable manifolds cannot intersect.

**B. Probabilistic analysis of the edge of chaos**

Since a complete characterization of the edge is not possible, due to its high dimensionality, a more practical way to study and describe it is by the following probabilistic approach. We calculate the probability that an initial condition with a given energy will lead to chaotic behavior by drawing sets of 2000 uniformly distributed initial conditions with the same energy from the surface of a nine-dimensional hypersphere whose radius is the square root of the initial energy in the system, which ranges from  $E(0) = 5 \times 10^{-5}$  to  $5 \times 10^{-3}$ . (See Ref. [23] for details of the algorithm for finding appropriate initial conditions.) We integrate these initial conditions for a sufficiently long time to determine whether or not they lead to a solution which exhibits chaotic behavior. Note that as  $\text{Re}$  increases, the time it takes for trajectories to reach the chaotic saddle (associated with transient chaos) also increases, so we increase the integration time as appropriate. For this analysis, we track the amplitude of the basic mode  $a_1$  as our indicator of chaotic behavior in the system. The laminar state corresponds to  $a_1 = 1$ , which differs significantly from the value of the amplitude in the chaotic saddle ( $a_1 \approx 0.5$ ). Therefore, we are able to determine if a trajectory becomes chaotic by monitoring whether  $a_1$  crosses the threshold  $a_1 = 0.5$ .

Figure 8 shows that the probability of transient chaos increases with Reynolds number and perturbation amplitude. We find that these probability curves agree well with the average value of the energy of the UPO associated with the edge of chaos. In particular, superimposing the average energy in the orbit on the contour plot, we see that the curve is in the 96%–97% probability range; see the thick black curve in Fig. 8. Furthermore, a scaling analysis determined that the contours scale as  $\sim \text{Re}^{-2}$ . This result agrees well with the Reynolds number scaling analysis performed for the UPO associated with the edge of chaos.

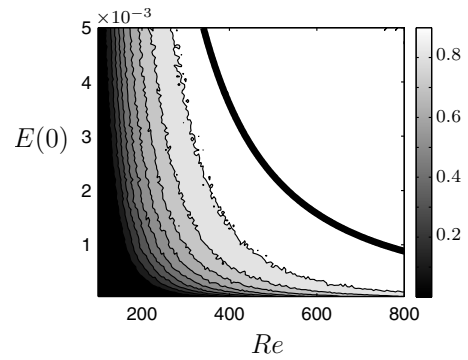


FIG. 8. Probability of transient chaos as a function of the Reynolds number and initial perturbation energy. The contour lines represent probability increments of 10% with the upper contour being the 90% curve. The thick black curve represents the average energy in the UPO associated with the edge of chaos.

**C. Basin boundary of the nontrivial attractor**

For  $335 \leq \text{Re} \leq 515$ , there is a coexisting stable, nontrivial attractor. In Ref. [15] it is shown that this attractor captures signatures of the self-sustaining process identified in Ref. [16,24,25]; for this reason, we associate the nontrivial attractor with sustained turbulence in this paper. The attractor can be chaotic (for  $335 \leq \text{Re} \leq 355$ ), periodic (for  $355 \leq \text{Re} \leq 508$ ), or quasiperiodic (for  $508 \leq \text{Re} \leq 515$ ), and in all cases explores similar regions of phase space; see Fig. 9. In Fig. 10, we show the time series for the evolution of the amplitude  $a_4$  for an initial condition near the laminar state fixed point for  $\text{Re} = 400$ . Recall that the laminar state has  $a_4 = 0$ . Here, the system again visits near the same UPO found in Fig. 3 (but for a different  $\text{Re}$  value), then displays transient chaotic behavior, and finally goes to the nontrivial attractor. This corresponds to the initial condition labelled  $c$  in Fig. 4. We found that initial conditions which give tran-

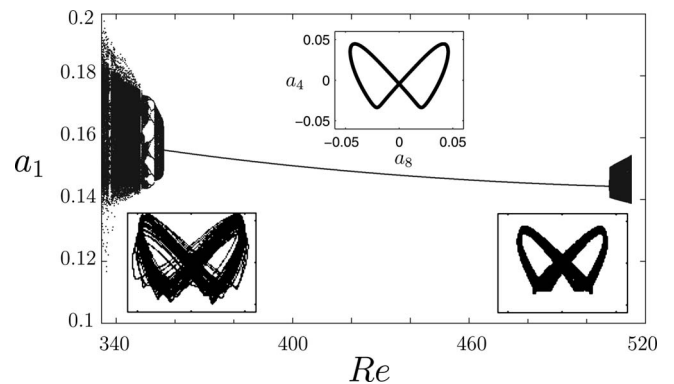


FIG. 9. Bifurcation diagram showing the instantaneous value of  $a_1$  whenever the trajectory pierces the Poincaré section defined by  $a_2 = 0$  with  $\dot{a}_2 < 0$ . This plot is generated by adiabatically changing the value of  $\text{Re}$ , omitting transients. For  $335 \leq \text{Re} \leq 355$ , the attractor is typically chaotic (shown in the bottom left inset for  $\text{Re} = 345$ ), for  $355 \leq \text{Re} \leq 508$  the attractor is a stable periodic orbit (shown in the top center inset for  $\text{Re} = 400$ ), and for  $508 \leq \text{Re} \leq 515$  the attractor is quasiperiodic (shown in the bottom right inset for  $\text{Re} = 510$ ) and in all cases explores similar regions in phase space. For more detail for  $335 \leq \text{Re} \leq 360$ , see Fig. 21 of Ref. [15].

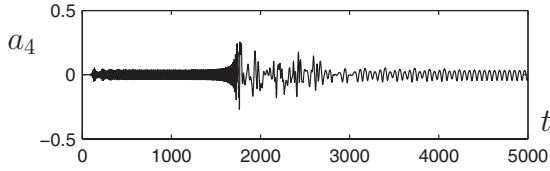


FIG. 10. Time evolution for the amplitude  $a_4$  for the nine-dimensional model at  $Re=400$  showing a qualitatively different behavior from Fig. 3 for an initial condition near the laminar state. Behaviors analogous to those shown in Fig. 3 occur for initial conditions which differ in  $a_4$  by a quantity of order  $10^{-15}$ .

sient chaos before decaying to the laminar state and initial conditions which give transient chaos before reaching the nontrivial attractor are extremely close together in phase space.

At  $Re \approx 515$ , the nontrivial attractor undergoes a crisis [26], and for higher  $Re$  it ceases to exist. This is apparently due to the boundary of the basin of attraction of the attractor colliding with one of the many unstable periodic orbits for this model, see Ref. [15]. This implies that all trajectories beyond this critical Reynolds number will eventually decay to the laminar state; however, they can display transient chaos before this decay. The situation for  $515 \leq Re < 1000$  is thus similar that of  $Re \leq 335$  and to the situation for a different low-dimensional model considered in Ref. [10].

Figure 11 shows the probability that perturbations of a given initial energy lead to the nontrivial attractor for  $335 \leq Re \leq 515$ . The first sharp contour line indicates a 10% probability of reaching the nontrivial attractor, and the last contour line corresponds to a 60% probability. Below  $Re \approx 335$ , there is no nontrivial attractor, and all trajectories approach the laminar state fixed point. A numerical scaling analysis shows that each of the contour lines in Fig. 11 scales as

$$E(0) = c(Re - Re_c)^\sigma, \tag{8}$$

where  $c$  is a constant whose value for this fit is always  $5 \times 10^{-3}$ . This fit has two important parameters:  $Re_c$  which is the Reynolds number to which the probability contours

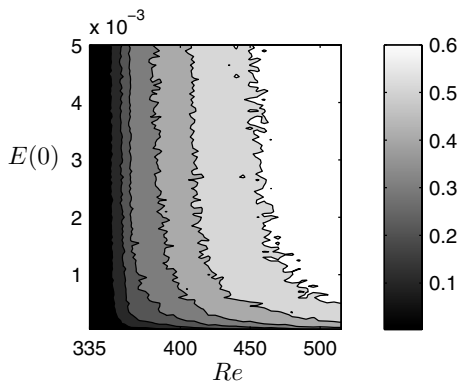


FIG. 11. Probability of reaching the nontrivial attractor associated with sustained turbulence as a function of the Reynolds number and initial perturbation energy.

asymptotically tend, and  $\sigma$  which is the scaling factor for each curve. We find  $Re_c = \{349, 357, 362, 380, 405, 450\}$  for the 10%–60% contours, respectively. The values of the scaling factor  $\sigma = \{-1.6, -1.3, -0.85, -0.73, -0.65, -0.55\}$  are comparable to the turbulent threshold exponent for other shear flows, such as PCF and plane Poiseuille flow; see, e.g., Refs. [27,28].

The relationship between the edge of chaos and the basin boundary is explored in Fig. 12, at  $Re=400$ . This figure shows that the stable manifold of the UPO associated with the edge of chaos smoothly and sharply separates (gray) direct decay to the laminar state from (black and white) transient chaotic behavior. This is in contrast to the basin structure between initial conditions which lead to the laminar state fixed point or the non-trivial attractor, as seen in the black and white speckled region in the figure. The basin boundary between these two behaviors, as shown in Fig. 12, is not smooth similar to the edge of chaos, but rather apparently fractal in nature. The fact that trajectories can come back to the laminar state after a chaotic transient is interesting. A possible explanation is that the stable manifold of the UPO could be a closed, nonorientable surface with neither an inside or an outside.

#### IV. TRANSIENT ENERGY GROWTH

It has been suggested that transient growth due to linear mechanisms is important for the transition to turbulence, since it can lead to large perturbations from the laminar state which may trigger nonlinear effects that lead to turbulence [1,27–30]. We investigate this issue for the present model by comparing the initial conditions which give the largest transient energy growth in the system and initial conditions which lie in the basin of attraction of the nontrivial attractor that we associate with sustained turbulence.

To do this, we define the dot product between the initial condition which gives the largest overall transient energy growth  $\mathbf{a}^{(TG)}$  and any initial condition  $\mathbf{a}$  with the same energy as

$$\Gamma(\mathbf{a}) = \frac{|\mathbf{a}^{(TG)} \cdot \mathbf{a}|}{|\mathbf{a}^{(TG)}|^2}. \tag{9}$$

Note that for this analysis, we normalize the vectors so that  $\Gamma \in [0, 1]$ . A large value for  $\Gamma$  indicates that the vectors are roughly parallel, while a small value indicates that they are almost perpendicular. Figure 13 shows probability density functions for initial conditions that have a particular value of  $\Gamma$  which are in the basin of attraction of the nontrivial attractor and for random initial conditions. For this analysis, we sampled 5000 random initial conditions uniformly distributed on spheres of constant perturbation energies  $E(0) = \{5 \times 10^{-5}, 5 \times 10^{-4}, 5 \times 10^{-3}\}$  and  $Re = \{400, 510\}$ . For all cases, the analysis suggests that initial conditions in the basin of attraction of the nontrivial attractor are correlated with the initial condition that yields the optimal transient energy growth. However, that correlation is only strong when the initial energy in the system is very small and diminishes as we move farther way from the laminar state.

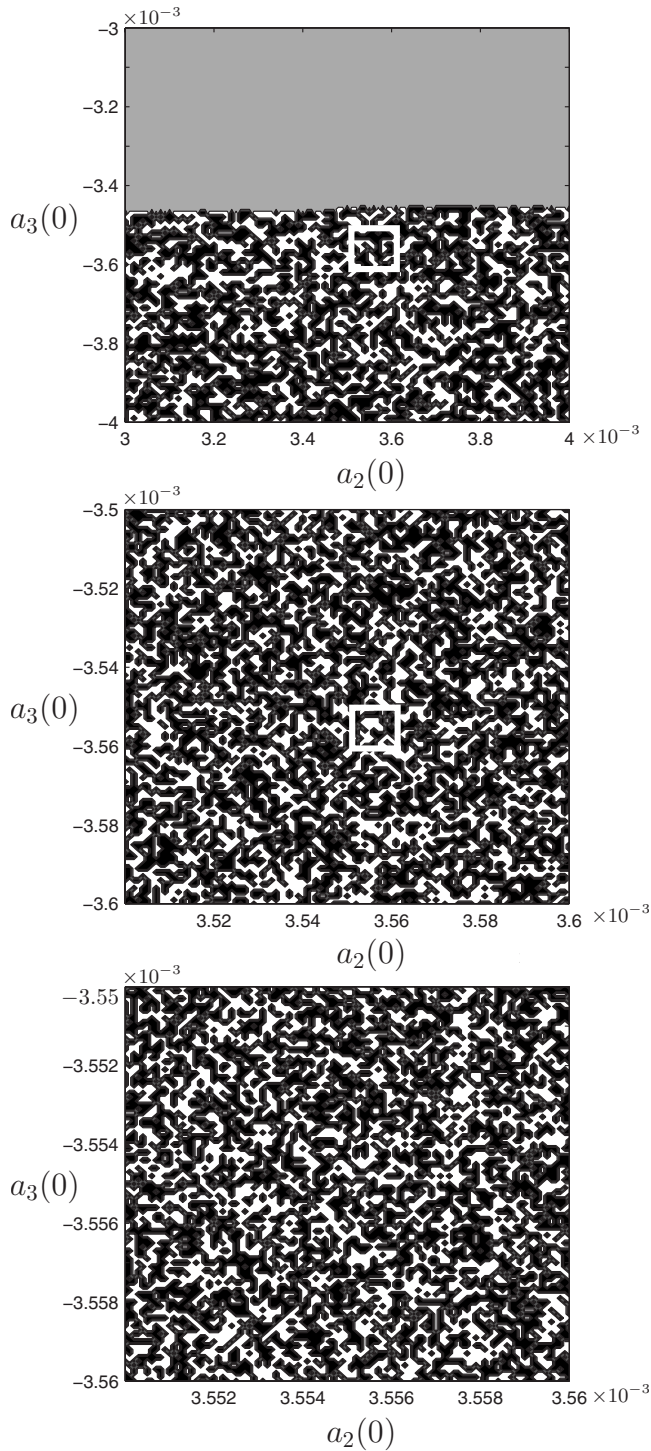


FIG. 12. A two-dimensional visualization of the edge of chaos showing initial conditions which (gray) directly decay to the laminar state, (black) become transiently chaotic before decaying to the laminar state, and (white) are transiently chaotic and then tend towards the nontrivial attractor corresponding the stable periodic orbit at  $Re=400$ . The center and bottom panels show successive magnifications.

However, many initial conditions are in the basin of attraction of the nontrivial attractor but do not point in the direction of the largest transient growth. This is illustrated in the velocity reconstructions shown in Fig. 14 for  $Re=400$ ,

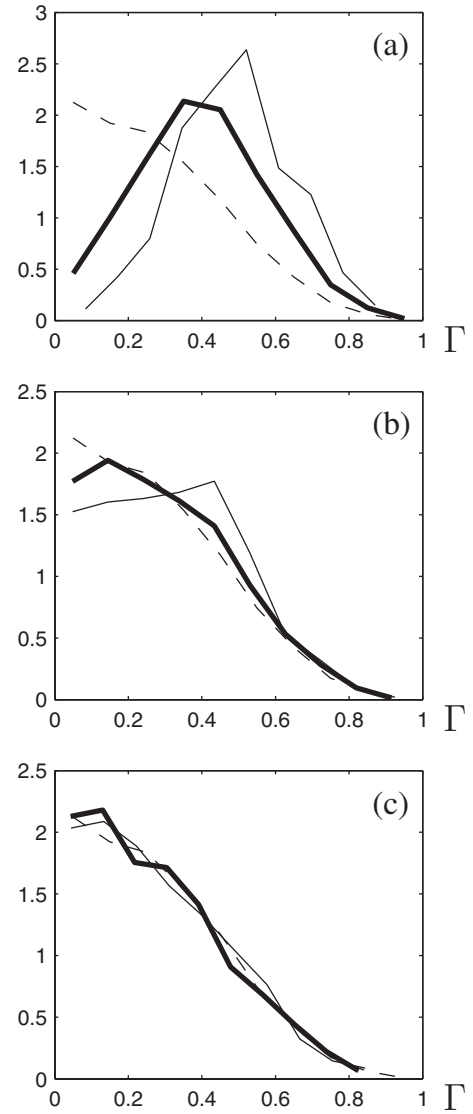


FIG. 13. Probability density functions for the dot product  $\Gamma$  between the initial condition which gives the largest overall transient growth and (dashed) any arbitrary initial condition, (solid) initial conditions in the basin of attraction of the nontrivial attractor for  $Re=400$ , (bold solid) initial conditions in the basin of attraction of the nontrivial attractor for  $Re=510$  for three different initial energies: (a)  $E(0)=5 \times 10^{-5}$ , (b)  $E(0)=5 \times 10^{-4}$ , (c)  $E(0)=5 \times 10^{-3}$ .

where the initial condition on the top is that which gives maximum transient growth (for the linearization about the laminar state), and the initial condition on the bottom is a typical one which lies in the basin of attraction of the nontrivial attractor. Both panels show the downstream vortices along half the length of the channel, where the velocity fields are represented by vectors for the components shown on the plane and the grayscale represents the streamwise velocity. We see that the initial condition with optimal transient growth has stronger streamwise vortices and weaker streaks, whereas the initial condition in the basin of attraction of the nontrivial attractor has the bulk of the energy in the streaks rather than the vortices.

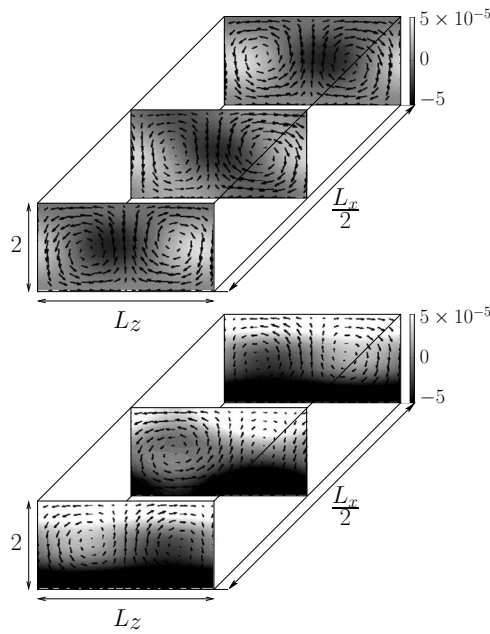


FIG. 14. Velocity fields along half the channel length for (top) the initial condition which gives the largest transient energy growth for the linearization about the laminar state and (bottom) a typical initial condition in the basin of attraction of the nontrivial attractor for  $Re=400$  and  $E(0)=5 \times 10^{-5}$ .

## V. CONCLUSION

The edge of chaos serves as a boundary between laminar and chaotic behavior, in the sense that initial conditions starting on one side directly decay to the laminar profile, and initial conditions on the other side exhibit transiently chaotic behavior. We characterized the edge of chaos for a nine-dimensional model for sinusoidal shear flow as the eight-

dimensional stable manifold of an unstable periodic orbit, whose properties were described in detail. For this model, for  $335 \leq Re \leq 515$  sustained turbulence is associated with a nontrivial attractor, which could be chaotic, a periodic orbit, or a quasiperiodic attractor. For  $515 \leq Re < 1000$ , there is no longer a nontrivial attractor and the stable manifold of the unstable periodic orbit associated with the edge of chaos separates initial conditions which directly decay to the laminar state from those which give a chaotic transient. Furthermore, we determined the probability that perturbations of a given energy lead to transient chaos before decay to the laminar state, or to a nontrivial attractor.

A scaling analysis of the probability that an initial condition with a particular energy and at a particular  $Re$  leads to a nontrivial attractor gave reasonable agreement with scalings for similar shear flows. We also found a correlation between initial conditions in the basin of attraction of the nontrivial attractor and the initial condition that yields optimal transient growth. However, there are many initial conditions which show only a weak correlation to optimal transient growth but still lead to the nontrivial attractor; indeed, many initial conditions leading to the nontrivial attractor have more energy in the streaks rather than the streamwise vortices, which contrasts with initial conditions for optimal transient growth which have more energy in the streamwise vortices than the streaks, cf. Ref. [31]. This provides evidence that the study of transient growth is of limited usefulness for understanding transition to turbulence.

## ACKNOWLEDGMENTS

This work was supported by the Alfred P. Sloan Foundation. The authors would like to thank Bruno Eckhardt for discussions about this work and the referees for their many useful comments.

- 
- [1] P. J. Schmid and D. S. Henningson, *Stability and Transition in Shear Flows* (Springer-Verlag, New York, 2000).
- [2] B. Eckhardt, T. M. B. Hof, and J. Westerweel, *Annu. Rev. Fluid Mech.* **39**, 447 (2007).
- [3] P. G. Drazin and W. H. Reid, *Hydrodynamic Stability* (Cambridge University Press, Cambridge, UK, 1981).
- [4] M. Nagata, *J. Fluid Mech.* **217**, 519 (1990).
- [5] R. M. Clever and F. H. Busse, *J. Fluid Mech.* **234**, 511 (1992).
- [6] A. Schmiegel, Ph.D. thesis, Universität Marburg, Marburg, 1999.
- [7] H. Faisst, Ph.D. thesis, Universität Marburg, Marburg, 2003.
- [8] B. Hof, C. W. H. van Doorne, J. Westerweel, F. T. M. Nieuwstadt, H. Faisst, B. Eckhardt, H. Wedin, R. R. Kerswell, and F. Waleffe, *Science* **305**, 1594 (2004).
- [9] J. Wang, J. F. Gibson, and F. Waleffe, *Phys. Rev. Lett.* **98**, 204501 (2007).
- [10] J. D. Skufca, J. A. Yorke, and B. Eckhardt, *Phys. Rev. Lett.* **96**, 174101 (2006).
- [11] T. M. Schneider, B. Eckhardt, and J. A. Yorke, *Phys. Rev. Lett.* **99**, 034502 (2007).
- [12] T. M. Schneider, B. Eckhardt, J. F. Gibson, M. Lagha, and F. de Lillo (unpublished).
- [13] Y. Duguet, A. P. Willis, and R. R. Kerswell, e-print arXiv:07111.2175.
- [14] J. Moehlis, H. Faisst, and B. Eckhardt, *New J. Phys.* **6**, 56 (2004).
- [15] J. Moehlis, H. Faisst, and B. Eckhardt, *SIAM J. Appl. Dyn. Syst.* **4**, 352 (2005).
- [16] F. Waleffe, *Phys. Fluids* **9**, 883 (1997).
- [17] T. R. Smith, J. Moehlis, and P. Holmes, *J. Fluid Mech.* **538**, 71 (2005).
- [18] J. Hamilton, J. Kim, and F. Waleffe, *J. Fluid Mech.* **287**, 317 (1995).
- [19] J. Moehlis, B. Eckardt, and H. Faisst, *Chaos* **14**, S11 (2004).
- [20] E. Doedel, A. Champneys, T. Fairgrieve, Y. Kuznetsov, B. Sandstede, and X. Wang, “*AUTO 97: Continuation and bifurcation software for ordinary differential equations (1997)*,” available from <http://indy.cs.concordia.ca/auto/>
- [21] M. Golubitsky, I. Stewart, and D. G. Schaeffer, *Singularities and Groups in Bifurcation Theory* (Springer-Verlag, New

- York, 1988), Vol. II.
- [22] J. Moehlis and E. Knobloch, scholarpedia. <http://www.scholarpedia.org>
- [23] L. Kim and J. Moehlis (unpublished).
- [24] F. Waleffe, *Stud. Appl. Math.* **95**, 319 (1995).
- [25] F. Waleffe, *Phys. Fluids* **7**, 3060 (1995).
- [26] C. Grebogi, E. Ott, and J. Yorke, *Physica D* **7**, 181 (1983).
- [27] L. N. Trefethen, A. E. Trefethen, S. Reddy, and T. Driscoll, *Science* **261**, 578 (1993).
- [28] S. J. Chapman, *J. Fluid Mech.* **451**, 35 (2002).
- [29] J. S. Baggett and L. N. Trefethen, *Phys. Fluids* **9**, 1043 (1997).
- [30] S. Grossmann, *Rev. Mod. Phys.* **72**, 603 (2000).
- [31] L. Kim and J. Moehlis, *Phys. Lett. A* **358**, 431 (2006).